Acta Mech
DOI 10.1007/s00707-010-0391-9

M. Lezgy-Nazargah · M. Shariyat · S. B. Beheshti-Aval

A refined high-order global-local theory for finite element bending and vibration analyses of laminated composite beams

Received: 19 July 2010 / Revised: 14 August 2010
© Springer-Verlag 2010

Abstract A refined high-order global-local laminated/sandwich beam theory is developed that satisfies all the kinematic and stress continuity conditions at the layer interfaces and considers effects of the transverse normal stress and transverse flexibility, e.g. for beams with soft cores or drastic material properties changes. The global displacement components, described by polynomial or combinations of polynomial and exponential expressions, are superposed on local ones chosen based on the layerwise or discrete-layer concepts. Furthermore, the non-zero conditions of the shear and normal tractions of the upper and lower surfaces of the beam may also be enforced. In the present C^1-continuous shear locking-free finite element model, the number of unknowns is independent of the number of layers. Comparison of present bending and vibration results for thin and thick beams with results of the three-dimensional theory of elasticity reveals efficiency of the present method. Moreover, the proposed model is computationally economic and has a high convergence rate.

1 Introduction

Due to their high specific strength and stiffness to weight ratios, laminated composite structures have been widely used in various mechanical and structural components, e.g. in space vehicles and smart structures with integrated piezoelectric sensors and actuators. Due to the discrete variations of the mechanical properties from a layer to the adjacent one, local variations of the stress distribution have to be determined accurately to avoid local failure phenomena such as delamination, matrix breakage and local excessive plastic deformations. Consequently, choosing an adequate mathematical model to accurately predict the local behaviors and performances of the mentioned structures under various environments is a key issue. Carrera and Brischetto [1], Zhang and Yang [2], and Hu et al. [3] have reviewed some theories that have been developed to investigate variations of the inter-laminar stresses of the laminated structures.

The most accurate approach to analyze the laminated plates/beams is solving the governing differential equations of the three-dimensional (3D) theory of elasticity [4–6]. However, the development of these solutions

M. Lezgy-Nazargah · S. B. Beheshti-Aval
Department of Civil Engineering, K.N. Toosi University of Technology, Tehran, Iran
E-mail: m.lezgy.n@gmail.com

S. B. Beheshti-Aval
E-mail: beheshti@kntu.ac.ir

M. Shariyat (✉)
Faculty of Mechanical Engineering, K.N. Toosi University of Technology,
Pardis Street, Molla-Sadra Avenue, Vanak Square, 19991 43344 Tehran, Iran
E-mail: m_shariyat@yahoo.com; shariyat@kntu.ac.ir

Published online: 26 October 2010

is a difficult task and the resulting solution cannot be expressed in a closed form for the general case of arbitrary geometry, boundary, and loading conditions. The computational 3D finite element analysis of these structures is expensive and, in some circumstances, not practical, especially when one dimension of the structure becomes much smaller than the other dimensions. These drawbacks encouraged some researchers to employ the two-dimensional (2D) models, prescribing variations of the displacement components in the transverse direction. This idea is the origin of all of the beam/plate theories. The differences among the available theories are mainly in the additional conditions that are employed to ensure that the prescribed transverse variations are accurate enough, especially when the number of layers increases or the differences in the material properties of the layers become significant. The available 2D theories in the literature can be classified into three broad groups: global or equivalent single layer theories (ESLT), local theories (e.g. layerwise (LWT) theories) and global-local theories.

Although in ESLT the number of the unknowns is independent of the number of layers, the transverse shear stress continuity condition in the interfaces of the layers is not guaranteed. Thus, in some circumstances, classical [7], Reissner-Mindlin-type first-order shear deformation [8–10] and third-order shear deformation [11] theories, which are variants of the ESLT, may lead to inaccurate results.

In order to overcome the drawbacks of the ESLT, the idea of LWT or discrete-layer theory was presented by some researchers [11–15]. The displacement field along the thickness of each ply was approximated by a piecewise continuous function. In spite of the fact that LWT reduces the restrictions of ESLT, in this type of theories the number of the unknowns is dependent on the number of layers, which in turn increases the computational cost of the analysis. To overcome this shortcoming, Heuer [16] employed a layerwise theory to study static and dynamic behaviors of the transversely isotropic, moderately thick sandwich beams imposing the continuity condition of the transverse shear stresses across the interfaces. Adam and Ziegler [17] presented a theory for predicting the elastic-plastic dynamic response of symmetrically designed composite beams with thick layers, assuming piecewise continuous and linear in-plane displacement fields through the layer thickness and defining an effective cross-sectional rotation. Moderately large vibrations of imperfect elastic-plastic composite beams with thick layers were analyzed by Adam [18]. Mindlin–Reissner kinematic assumptions were implemented layerwise, and Berger's approximation of the von Karman nonlinear strain–displacement relations was used. Adam [19] studied the nonlinear response of doubly curved panels composed of three thick isotropic layers subjected to time-varying lateral loads, employing a first-order layerwise theory which includes the transverse shear flexibility, initial geometric imperfections and Berger-type geometric nonlinearities.

In order to improve the accuracy of the results and reduce the number of the unknowns for the multilayered composites, zigzag (ZZ) theories were proposed by some researchers. These theories are able to reproduce piecewise continuous displacement and transverse stress fields in the thickness direction of the laminated structures. The first ZZ theory was proposed by Lekhnitskii [20] for multi-layered beams. Ren [21,22] extended Lekhnitskii's theory to orthotropic and anisotropic layered plates. ZZ theories were used and developed by Ambartsumyan [23], Whitney [24], Icardi [25–27], Reissner [28], Murakami [29,30] and Carrera [31,32]. Vidal and Polit [33] and Beheshti-Aval and Lezgy-Nazargah [34] presented ZZ theories for the analysis of laminated beams based on sine functions. An excellent review in the ZZ theories has been introduced by Carrera [35].

Based on the double superposition of the local components of the in-plane displacements on the global ones, Li and Liu [36] proposed the first global-local laminate theory. Using this theory, the in-plane stresses and transverse shear stresses can be well estimated from the constitutive equations. Shariyat [37–39] extended the double superposition theory of Li and Liu and proposed a generalized global-local higher-order theory for the composite laminates. This generalized global-local higher-order theory satisfies the transverse shear and normal stresses continuity at the interfaces and is calibrated based on the general nonlinear Green's strain tensor.

The transverse normal stresses and strains and the transverse flexibility, which are the cause of many failure modes such as wrinkling and delamination, have important roles in the analysis of the laminated/sandwich structures, especially those with soft cores. However, the majority of the 2D theories ignores the transverse normal stress and strain and the transverse flexibility (e.g. to avoid Poisson's thickness locking [40] occurrence). Thus, in these theories the transverse normal stress cannot be calculated directly from the constitutive equations, and prediction of this stress requires integration of the equilibrium equations in the transverse direction. The majority of the available ZZ theories either does not consider the transverse flexibility or does not impose the continuity condition of the transverse normal stress at the interfaces [41,42].

With the exception of some limited theories, e.g. the generalized global-local higher-order theory of Shariyat [37–39], the available global-local laminated beam/plate theories have discarded influences of the transverse

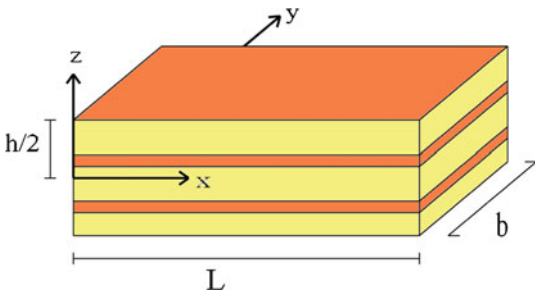

Fig. 1 Geometric parameters of the laminated beam

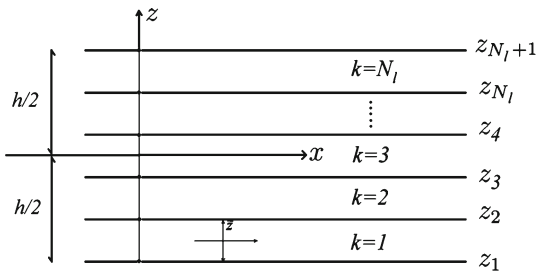

Fig. 2 Global and local coordinate systems of the laminated beam

flexibility and the transverse normal stress. To overcome restrictions of the available theories, in the present study a novel refined global-local laminate theory is presented based on the superposition hypothesis for bending and vibration analyses of the laminated/sandwich composite beams. In the proposed theory, the global in-plane displacement components are described by combinations of polynomial and exponential expressions whereas the global transverse displacement component is adopted as a fourth-order polynomial. To improve the results, local terms have been added to the global expressions employing either the layerwise or discrete-layer concepts. The boundary conditions of the shear and normal tractions are satisfied on the upper and lower surfaces of the beam. Besides, continuity conditions of the displacement components, transverse shear and normal stresses, and the transverse normal stress gradient at the layer interfaces are satisfied. In comparison with the other available similar theories (the generalized global-local theory of Shariyat [37–39] and LWT or 3D models employed in the commercial softwares), the present model is computationally significantly economic and has only four independent generalized unknown parameters (three displacement and one rotation parameters).

Based on the proposed model, a three-nodded shear locking-free beam element with C^0-continuity for the in-plane displacements and C^1-continuity for the in-plane variations of the lateral deflection is employed. Various bending and vibration validation examples are treated using a written computer code whose algorithm is based on the present model. Having some additional advantages, the obtained numerical results exhibit good agreements with the available published and the 3D finite element results.

2 Theoretical formulations of the proposed global-local theory

2.1 The geometric parameters and the coordinate system of the beam

The considered beam is a prismatic one with a rectangular uniform cross section of height h and width b. The beam is made of N_l layers of different linearly elastic composite materials. The geometric parameters of the laminated beam and the chosen Cartesian coordinate system (x, y, z) are shown in Fig. 1. As it may be noted from Fig. 1, the x, y and z axes are respectively along the length, width and thickness of the beam. Since it is intended to develop a global-local beam theory, transverse global and local coordinate systems shown in Fig. 2 are chosen to present the beam model.

2.2 The constitutive equations

The stress–strain relations of each orthotropic layer of the laminate can be expressed as:

$$\boldsymbol{\sigma}^{(k)} = \boldsymbol{C}^{(k)}\boldsymbol{\varepsilon}^{(k)} \tag{1}$$

where k denotes the layer number and:

$$\boldsymbol{\sigma}^{(\mathrm{k})} = \begin{bmatrix} \sigma_{11}^{(k)} \\ \sigma_{33}^{(k)} \\ \tau_{13}^{(k)} \end{bmatrix}, \quad \boldsymbol{\varepsilon}^{(\mathrm{k})} = \begin{bmatrix} \varepsilon_{11}^{(k)} \\ \varepsilon_{33}^{(k)} \\ \gamma_{13}^{(k)} \end{bmatrix}, \quad \boldsymbol{C}^{(k)} = \begin{bmatrix} c_{11}^{(k)} & c_{13}^{(k)} & 0 \\ c_{13}^{(k)} & c_{33}^{(k)} & 0 \\ 0 & 0 & c_{55}^{(k)} \end{bmatrix}$$

and $c_{ij}^{(k)}$ are the elastic coefficients.

2.3 The displacement field description

In the present study, the following global-local displacement field is proposed ($k = 1, 2, \ldots, N_l$):

$$\begin{aligned} u^k(x,y,z,t) &= u_0(x,t) - zw(x,t)_{,x} + ze^{-2(z/h)^2}\left[\theta(x,t) + w(x,t)_{,x}\right] + \bar{u}_L^k(x,z,t) + \hat{u}_L^k(x,z,t), \\ w^k(x,y,z,t) &= w_0(x,t) + zw_1(x,t) + z^2w_2(x,t) + z^3w_3(x,t) + z^4w_4(x,t) \\ &\quad + \sum_{i=1}^{k-1}\psi_i(x,t)(z - z_{i+1})H(z - z_{i+1}) + \sum_{i=1}^{k-1}\Psi_i(x,t)(z - z_{i+1})^2H(z - z_{i+1}) \end{aligned} \tag{2}$$

where H is Heaviside's function. The functions $u(x, y, z, t)$ and $w(x, y, z, t)$ represent the horizontal (in-plane) and vertical (transverse) displacement components, respectively. The $u_0(x,t)$, $w_0(x,t)$, $w_1(x,t)$, $w_2(x,t)$, $w_3(x,t)$ and $w_4(x,t)$ are global displacement parameters of the reference layer (e.g. the first layer). t is time and $\theta(x,t)$ denotes the shear-bending rotation around the y axis. $\psi_i(x,t)$ and $\Psi_i(x,t)$ are functions to be determined in order to fulfill the transverse normal stress and stress gradient continuity conditions at the laminate interfaces. The local components $\bar{u}_L^k$ and $\hat{u}_L^k$ can be chosen based on the layerwise variations concept. Therefore, if they are chosen as combinations of the Legendre polynomials to simplify the numerical integration process, one may write:

$$\bar{u}_L^k(x,z,t) = \bar{z}_k u_1^k(x,t) + \frac{3\bar{z}_k^2 - 1}{2}u_2^k(x,t), \tag{3}$$

$$\hat{u}_L^k(x,z,t) = \frac{5\bar{z}_k^3 - 3\bar{z}_k}{2}u_3^k(x,t) \tag{4}$$

where $\bar{z}_k = a_k z - b_k$, $a_k = \frac{2}{z_{k+1} - z_k}$, $b_k = \frac{z_{k+1} + z_k}{z_{k+1} - z_k}$.

Local variations of the transverse displacement component are represented by the two summations appearing in Eq. (2), employing a discrete-layer concept [43].

The continuity conditions of the displacement components at the laminate interfaces should be satisfied. Due to using a layerwise description for the local term, the transverse displacement component satisfies the kinematic continuity condition automatically. By imposing the continuity conditions of the in-plane displacement component, the following two equations are obtained:

$$\bar{u}_L^k = \bar{u}_L^{k-1}, \quad k = 2, \ldots, N_l, \tag{5}$$

$$\hat{u}_L^k = \hat{u}_L^{k-1}, \quad k = 2, \ldots, N_l. \tag{6}$$

Equations (5) and (6) lead to the following equations:

$$u_2^k = u_1^{k-1} + u_2^{k-1} + u_1^k, \tag{7}$$

$$u_3^k = (-1)^{k-1}u_3^1. \tag{8}$$

Since ZZ models based on the constant transverse displacement assumption have been capable of estimating the transverse shear stress satisfactorily from the constitutive equations [23–25,33], the simplifying assumption $w(x, y, z, t) = w_0(x, t)$ is used in computation of the transverse shear stress only to avoid the computational complexity. Hence, the transverse shear stress of the *k-th* layer may be determined from the following equation:

$$\tau_{xz}^{(k)} = G_k \left(e^{-2(z/h)^2} - 4 \left(\frac{z}{h} \right)^2 e^{-2(z/h)^2} \right) (\theta + w_{0,x}) + G_k a_k u_1^k + 3 G_k \bar{z}_k a_k u_2^k + G_k \left(-\frac{3}{2} a_k + \frac{15}{2} a_k \bar{z}_k^2 \right) u_3^k \tag{9}$$

where $G_k = c_{55}^{(k)}$ is the transverse shear modulus of the kth layer. By imposing the transverse shear stress continuity condition at the mutual interfaces of the adjacent layers, the following recursive condition is obtained:

$$\begin{aligned} & G_k \left(e^{-2(z_k/h)^2} - 4 \left(\frac{z_k}{h} \right)^2 e^{-2(z_k/h)^2} \right) (\theta + w_{0,x}) + G_k a_k u_1^k - 3 G_k a_k u_2^k + 6 G_k a_k u_3^k \\ & = G_{k-1} \left(e^{-2(z_k/h)^2} - 4 \left(\frac{z_k}{h} \right)^2 e^{-2(z_k/h)^2} \right) (\theta + w_{0,x}) + G_{k-1} a_{k-1} u_1^{k-1} \\ & \quad + 3 G_{k-1} a_{k-1} u_2^{k-1} + 6 G_{k-1} a_{k-1} u_3^{k-1}. \end{aligned} \tag{10}$$

Furthermore, the boundary conditions of the prescribed values of the shear tractions (that are generally non-zero values) on the top and bottom surfaces of the beam should be satisfied. Thus, the following two boundary conditions are obtained:

$$\tau_{xz}^{(1)} \left(z = -\frac{h}{2} \right) = G_1 a_1 u_1^1 - 3 G_1 a_1 u_2^1 + 6 G_1 a_1 u_3^1 = X^-(x, t), \tag{11}$$

$$\tau_{xz}^{(N_l)} \left(z = \frac{h}{2} \right) = G_{N_l} a_{N_l} u_1^{N_l} + 3 G_{N_l} a_{N_l} u_2^{N_l} + 6 G_{N_l} a_{N_l} u_3^{N_l} = X^+(x, t) \tag{12}$$

where $X^-(x, t)$ and $X^+(x, t)$ are the prescribed shear tractions of the bottom and top surfaces of the beam, respectively. By using Eqs. (7) and (10), the following recursive equations are obtained:

$$u_1^k = A_k (\theta + w_{0,x}) + B_k u_1^{k-1} + C_k u_2^{k-1} + D_k u_3^k, \tag{13}$$

$$u_2^k = E_k (\theta + w_{0,x}) + F_k u_1^{k-1} + H_k u_2^{k-1} + I_k u_3^k \tag{14}$$

where the coefficients A_k, B_k, C_k, D_k, E_k, F_k, H_k and I_k are:

$$\begin{aligned} A_k &= \frac{\left(e^{-2(z_k/h)^2} - 4(z_k/h)^2 e^{-2(z_k/h)^2} \right) (G_k - G_{k-1})}{2 G_k a_k}, \quad B_k = \frac{(-G_{k-1} a_{k-1} - 3 G_k a_k)}{2 G_k a_k}, \\ C_k &= \frac{(-3 G_{k-1} a_{k-1} - 3 G_k a_k)}{2 G_k a_k}, \quad D_k = \frac{(6 G_{k-1} a_{k-1} + 6 G_k a_k)}{2 G_k a_k}, \quad E_k = A_k, \\ F_k &= \frac{(-G_{k-1} a_{k-1} - G_k a_k)}{2 G_k a_k}, \quad H_k = \frac{(-3 G_{k-1} a_{k-1} - G_k a_k)}{2 G_k a_k}, \quad I_k = D_k. \end{aligned} \tag{15}$$

Substituting Eq. (8) into Eq. (11) yields:

$$u_3^k = \frac{(-1)^{k-1} X^-}{6 G_1 a_1} + \frac{(-1)^k}{6} u_1^1 + \frac{(-1)^{k-1}}{2} u_2^1. \tag{16}$$

The above equation expresses u_3^k in terms of u_1^1, u_2^1 and X^-. Substituting Eq. (16) into the recursive Eqs. (13) and (14) relates u_1^k and u_2^k to u_1^1, u_2^1, $(\theta + w_{0,x})$ and X^-. After calculating $u_1^{N_l}$, $u_2^{N_l}$ and $u_3^{N_l}$ from the recursive Eqs. (13), (14) and (16), respectively, and substituting them into Eq. (12), u_2^1 can be eliminated. Thus Eqs. (13), (14) and (16) can be rewritten as:

$$\begin{aligned} u_1^k(x, t) &= \alpha_1^k \left(\theta(x, t) + w_0(x, t)_{,x} \right) + \beta_1^k u_1^1(x, t) + \delta_1^k X^+(x, t) + \lambda_1^k X^-(x, t), \\ u_2^k(x, t) &= \alpha_2^k \left(\theta(x, t) + w_0(x, t)_{,x} \right) + \beta_2^k u_1^1(x, t) + \delta_2^k X^+(x, t) + \lambda_2^k X^-(x, t), \\ u_3^k(x, t) &= \alpha_3^k \left(\theta(x, t) + w_0(x, t)_{,x} \right) + \beta_3^k u_1^1(x, t) + \delta_3^k X^+(x, t) + \lambda_3^k X^-(x, t) \end{aligned} \tag{17}$$

where the coefficients α_1^k, α_2^k, α_3^k, β_1^k, β_2^k, β_3^k, δ_1^k, δ_2^k, δ_3^k, λ_1^k, λ_2^k, λ_3^k are obtained from the procedure described above. These coefficients are only dependent on the shear modulus and the global coordinates of the layers.

The transverse normal stress and stress gradient within the *k-th* layer may be determined from the following equations:

$$\begin{aligned}\sigma_{zz}^{(k)} &= c_{13}^{(k)}\varepsilon_{xx}^{(k)}+c_{33}^{(k)}\varepsilon_{zz}^{(k)} = c_{13}^{(k)}(u_{0,x}-zw_{0,xx}+(\theta_{,x}+w_{,xx})J(z)+T(z)u_{1,x}^1+P(z)(X^+)_{,x}+R(z)(X^-)_{,x})\\ &+c_{33}^{(k)}\left(w_1+2zw_2+3z^2w_3+4z^3w_4+\sum_{i=1}^{k-1}\psi_i H(z-z_{i+1})+2\sum_{i=1}^{k-1}\Psi_i(z-z_{i+1})H(z-z_{i+1})\right),\end{aligned} \tag{18}$$

$$\begin{aligned}\sigma_{zz,z}^{(k)} &= c_{13}^{(k)}(-w_{0,xx}+(\theta_{,x}+w_{0,xx})J(z)_{,z}+T(z)_{,z}u_{1,x}^1+P(z)_{,z}(X^+)_{,x}+R(z)_{,z}(X^-)_{,x})\\ &+c_{33}^{(k)}\left(2w_2+6zw_3+12z^2w_4+2\sum_{i=1}^{k-1}\Psi_i H(z-z_{i+1})\right)\end{aligned} \tag{19}$$

where

$$\begin{aligned}J(z) &= ze^{-2(z/h)^2}+\sum_{k=1}^{N_l}\left(\bar{z}_k\alpha_1^k+\left(-\frac{1}{2}+\frac{3\bar{z}_k^2}{2}\right)\alpha_2^k+\left(-\frac{3\bar{z}}{2}+\frac{5\bar{z}_k^3}{2}\right)\alpha_3^k\right)(H(z-z_k)-H(z-z_{k+1}))\,,\\ T(z) &= \sum_{k=1}^{N_l}\left(\bar{z}_k\beta_1^k+\left(-\frac{1}{2}+\frac{3\bar{z}_k^2}{2}\right)\beta_2^k+\left(-\frac{3\bar{z}}{2}+\frac{5\bar{z}_k^3}{2}\right)\beta_3^k\right)\times(H(z-z_k)-H(z-z_{k+1}))\,,\\ P(z) &= \sum_{k=1}^{N_l}\left(\bar{z}_k\delta_1^k+\left(-\frac{1}{2}+\frac{3\bar{z}_k^2}{2}\right)\delta_2^k+\left(-\frac{3\bar{z}}{2}+\frac{5\bar{z}_k^3}{2}\right)\delta_3^k\right)\times(H(z-z_k)-H(z-z_{k+1}))\,,\\ R(z) &= \sum_{k=1}^{N_l}\left(\bar{z}_k\lambda_1^k+\left(-\frac{1}{2}+\frac{3\bar{z}_k^2}{2}\right)\lambda_2^k+\left(-\frac{3\bar{z}}{2}+\frac{5\bar{z}_k^3}{2}\right)\lambda_3^k\right)\times(H(z-z_k)-H(z-z_{k+1}))\end{aligned} \tag{20}$$

and $H(z)$ denotes Heaviside's function.

Continuity of $\sigma_{zz,z}$ and σ_{zz} must be fulfilled at N_l-1 interfaces:

$$\sigma_{zz,z}^{(k+1)}(z_{k+1}) = \sigma_{zz,z}^{(k)}(z_{k+1}),\quad k=1,2,\ldots,N_l-1, \tag{21}$$

$$\sigma_{zz}^{(k+1)}(z_{k+1}) = \sigma_{zz}^{(k)}(z_{k+1}),\quad k=1,2,\ldots,N_l-1. \tag{22}$$

From the recursive Eqs. (21) and (22), $\psi_k(x,t)$ and $\Psi_k(x,t)$ will have the following form ($k=1,2,\ldots,N_l-1$):

$$\Psi_k = A_1^k w_{0,xx}+A_2^k w_2+A_3^k w_3+A_4^k w_4+A_5^k\theta_{,x}+A_6^k(u_1^1)_{,x}+A_7^k(X^+)_{,x}+A_8^k(X^-)_{,x}, \tag{23}$$

$$\psi_k = B_1^k w_{0,xx}+B_2^k w_1+B_3^k w_2+B_4^k w_3+B_5^k w_4+B_6^k(u_0)_{,x}+B_7^k\theta_{,x}+B_8^k(u_1^1)_{,x}+B_9^k(X^+)_{,x}+B_{10}^k(X^-)_{,x}. \tag{24}$$

Moreover, the boundary conditions of the transverse normal stress and transverse normal stress gradient on the upper and lower faces of the beam must be satisfied:

$$\sigma_{zz,z}^{(N_l)}(z_{N_l+1}) = \sigma_{zz,z}^{(1)}(z_1) = 0, \tag{25}$$

$$\sigma_{zz}^{(1)}(z_1) = Z^-(x,t),\ \sigma_{zz}^{(N_l)}(z_{N_l+1}) = Z^+(x,t) \tag{26}$$

where $Z^-(x,t)$ and $Z^+(x,t)$ are the distributed lateral loads acting on the bottom and top surfaces of the beam, respectively. From Eqs. (25) and (26), the unknowns w_1, w_2, w_3 and w_4 can be expressed in terms of $u_{0,x}$, $w_{0,xx}$, $\theta_{,x}$, $(u_1^1)_{,x}$, $(X^+)_{,x}$, $(X^+)_{,x}$, Z^+, and Z^-:

$$w_1(x,t) = \Theta_{11}(u_0)_{,x}+\Theta_{12}w_{0,xx}+\Theta_{13}\theta_{,x}+\Theta_{14}(u_1^1)_{,x}+\Theta_{15}(X^+)_{,x}+\Theta_{16}(X^-)_{,x}+\Theta_{17}Z^+ +\Theta_{18}Z^-, \tag{27}$$

$$w_2(x,t) = \Theta_{21}(u_0)_{,x}+\Theta_{22}w_{0,xx}+\Theta_{23}\theta_{,x}+\Theta_{24}(u_1^1)_{,x}+\Theta_{25}(X^+)_{,x}+\Theta_{26}(X^-)_{,x}+\Theta_{27}Z^+ +\Theta_{28}Z^-, \tag{28}$$

$$w_3(x,t) = \Theta_{31}(u_0)_{,x}+\Theta_{32}w_{0,xx}+\Theta_{33}\theta_{,x}+\Theta_{34}(u_1^1)_{,x}+\Theta_{35}(X^+)_{,x}+\Theta_{36}(X^-)_{,x}+\Theta_{37}Z^+ +\Theta_{38}Z^-, \tag{29}$$

$$w_4(x,t) = \Theta_{41}(u_0)_{,x}+\Theta_{42}w_{0,xx}+\Theta_{43}\theta_{,x}+\Theta_{44}(u_1^1)_{,x}+\Theta_{45}(X^+)_{,x}+\Theta_{46}(X^-)_{,x}+\Theta_{47}Z^+ +\Theta_{48}Z^-. \tag{30}$$

By substituting Eqs. (27) to (30) into Eqs. (23) and (24), $\psi_i(x,t)$ and $\Psi_i(x,t)$ can be rewritten as follows ($k = 1, 2, \ldots, N_l - 1$):

$$\Psi_i(x,t) = C_1^i(u_0)_{,x} + C_2^i w_{0,xx} + C_3^i\theta_{,x} + C_4^i(u_1^1)_{,x} + C_5^i(X^+)_{,x} + C_6^i(X^-)_{,x} + C_7^i Z^+ + C_8^i Z^-, \tag{31}$$

$$\psi_i(x,t) = D_1^i(u_0)_{,x} + D_2^i w_{0,xx} + D_3^i\theta_{,x} + D_4^i(u_1^1)_{,x} + D_5^i(X^+)_{,x} + D_6^i(X^-)_{,x} + Di\, Z^+ + D_8^i Z^-. \tag{32}$$

Finally, the expression of the transverse displacement takes the following form:

$$\begin{aligned} w^k(x,y,z,t) = w_0(x,t) &+ \Delta_1^k(z)u_{0,x} + \Delta_2^k(z)w_{0,xx} + \Delta_3^k(z)\theta_{,x} + \Delta_4^k(z)(u_1^1)_{,x} + \Delta_5^k(z)(X^+)_{,x} \\ &+ \Delta_6^k(z)(X^-)_{,x} + \Delta_7^k(z)Z^+ + \Delta_8^k(z)Z^- \end{aligned} \tag{33}$$

where

$$\Delta_1^k(z) = \Theta_{11}z + \Theta_{21}z^2 + \Theta_{31}z^3 + \Theta_{41}z^4 + \sum_{i=1}^{k-1} D_1^i(z - z_{i+1})H(z - z_{i+1}) + \sum_{i=1}^{k-1} C_1^i(z - z_{i+1})^2 H(z - z_{i+1}),$$

$$\Delta_2^k(z) = \Theta_{12}z + \Theta_{22}z^2 + \Theta_{32}z^3 + \Theta_{42}z^4 + \sum_{i=1}^{k-1} D_2^i(z - z_{i+1})H(z - z_{i+1}) + \sum_{i=1}^{k-1} C_2^i(z - z_{i+1})^2 H(z - z_{i+1}),$$

$$\Delta_3^k(z) = \Theta_{13}z + \Theta_{23}z^2 + \Theta_{33}z^3 + \Theta_{43}z^4 + \sum_{i=1}^{k-1} D_3^i(z - z_{i+1})H(z - z_{i+1}) + \sum_{i=1}^{k-1} C_3^i(z - z_{i+1})^2 H(z - z_{i+1}),$$

$$\Delta_4^k(z) = \Theta_{14}z + \Theta_{24}z^2 + \Theta_{34}z^3 + \Theta_{44}z^4 + \sum_{i=1}^{k-1} D_4^i(z - z_{i+1})H(z - z_{i+1}) + \sum_{i=1}^{k-1} C_4^i(z - z_{i+1})^2 H(z - z_{i+1}),$$

$$\Delta_5^k(z) = \Theta_{15}z + \Theta_{25}z^2 + \Theta_{35}z^3 + \Theta_{45}z^4 + \sum_{i=1}^{k-1} D_5^i(z - z_{i+1})H(z - z_{i+1}) + \sum_{i=1}^{k-1} C_5^i(z - z_{i+1})^2 H(z - z_{i+1}),$$

$$\Delta_6^k(z) = \Theta_{16}z + \Theta_{26}z^2 + \Theta_{36}z^3 + \Theta_{46}z^4 + \sum_{i=1}^{k-1} D_6^i(z - z_{i+1})H(z - z_{i+1}) + \sum_{i=1}^{k-1} C_6^i(z - z_{i+1})^2 H(z - z_{i+1}),$$

$$\Delta_7^k(z) = \Theta_{17}z + \Theta_{27}z^2 + \Theta_{37}z^3 + \Theta_{47}z^4 + \sum_{i=1}^{k-1} D_7^i(z - z_{i+1})H(z - z_{i+1}) + \sum_{i=1}^{k-1} C_7^i(z - z_{i+1})^2 H(z - z_{i+1}),$$

$$\Delta_8^k(z) = \Theta_{18}z + \Theta_{28}z^2 + \Theta_{38}z^3 + \Theta_{48}z^4 + \sum_{i=1}^{k-1} D_8^i(z - z_{i+1})H(z - z_{i+1}) + \sum_{i=1}^{k-1} C_8^i(z - z_{i+1})^2 H(z - z_{i+1}).$$

At this stage, all the unknowns of the proposed global-local displacement fields (Eq. (2)) are determined only in terms of four independent unknown parameters u_0, w_0, θ and u_1^1.

Using Cauchy's definition of the strain tensor, the in-plane, transverse shear and normal strain components may be calculated based on the proposed global-local description of the displacement field as:

$$\begin{aligned} \varepsilon_{xx} &= u_{0,x} - zw_{0,xx} + (\theta_{,x} + w_{0,xx})J(z) + T(z)u_{1,x}^1 + P(z)(X^+)_{,x} + R(z)(X^-)_{,x}, \\ \varepsilon_{zz} &= \Delta_1^k(z)_{,z}u_{0,x} + \Delta_2^k(z)_{,z}w_{0,xx} + \Delta_3^k(z)_{,z}\theta_{,x} + \Delta_4^k(z)_{,z}(u_1^1)_{,x} \\ &\quad + \Delta_5^k(z)_{,z}(X^+)_{,x} + \Delta_6^k(z)_{,z}(X^-)_{,x} + \Delta_7^k(z)_{,z}Z^+ + \Delta_8^k(z)_{,z}Z^-, \\ \gamma_{xz} &= (\theta + w_{0,x})J(z)_{,z} + T(z)_{,z}u_1^1 + P(z)_{,z}X^+ + R(z)_{,z}X^-. \end{aligned} \tag{34}$$

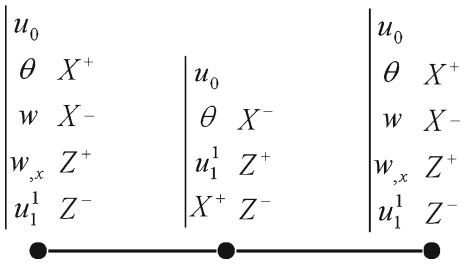

Fig. 3 Representation of the proposed laminated beam element as well as its degrees of freedom

Since the functions $u(x, y, z, t)$ and $w(x, y, z, t)$are coupled in the strain energy expression, it is expected that the presented global-local theory compensates to some extent for the simplifying assumption $w(x, y, z, t) = w_0(x, , t)$ used only in computation of the transverse shear stress.

3 The governing equations of the beam element

Using appropriate shape functions and nodal variables, a finite element representation of the displacement field description given in Eq. (2) may be introduced. It is known that the order of the differentiation operators of w_0 in the expression of the strain energy is higher in comparison with the remaining displacement components [44–47]. Moreover, for more accurate results, the slope continuity of the beam must be guaranteed. For these reasons, the in-plane variations of the transverse displacement component, w_0, must be C^1-continuous. Therefore, compatible Hermite cubic shape functions may be employed to interpolate the in-plane variations of the transverse displacement component w_0. The rotation θ can be C^0-continuous but it is interpolated by quadratic Lagrangian shape functions to ensure obtaining more accurate results. Furthermore, if identical orders are adopted for the shape functions of $w_{0,x}$ and θ parameters in the relevant transverse shear strain components, the shear locking phenomenon may be avoided due to using a consistent displacement field [33,35,48]. Finally, u_0, u_1^1, X^+, X^-, Z^+ and Z^- may be interpolated using Lagrangian quadratic shape functions. The proposed laminated beam element as well as its nodal degrees of freedom are shown in Fig. 3. Both the transverse shear stresses of the top and bottom layers and the displacement parameters are defined at the nodal points of the element. Therefore, interlaced discretization meshes are employed to present a mixed formulation (in the global sense). Therefore, based on Eqs. (2), (17), (33) and (34), the displacement and strain components may be expressed in the following form:

$$\boldsymbol{u} = \boldsymbol{A}_u \boldsymbol{u}_u, \quad \boldsymbol{\varepsilon} = \boldsymbol{L}_u \boldsymbol{u}_u \tag{35}$$

where $\boldsymbol{u} = \begin{bmatrix} u & w \end{bmatrix}^T$, $\boldsymbol{u}_u = \begin{bmatrix} u_0 & w_0 & \theta & u_1^1 & X^+ & X^- & Z^+ & Z^- \end{bmatrix}^T$, $\boldsymbol{\varepsilon} = \begin{bmatrix} \varepsilon_{xx} & \varepsilon_{zz} & \gamma_{xz} \end{bmatrix}^T$, and

$$\boldsymbol{A}_u = \begin{bmatrix} 1 & -z\frac{d}{dx} + J(z) & J(z) & T(z) & P(z) & R(z) & 0 & 0 \\ \Delta_1^k(z)\frac{d}{dx} & 1 + \Delta_2^k(z)\frac{d^2}{dx^2} & \Delta_3^k(z)\frac{d}{dx} & \Delta_4^k(z)\frac{d}{dx} & \Delta_5^k(z)\frac{d}{dx} & \Delta_6^k(z)\frac{d}{dx} & \Delta_7^k(z) & \Delta_8^k(z) \end{bmatrix},$$

$$\boldsymbol{L}_u = \begin{bmatrix} \frac{d}{dx} & -z\frac{d^2}{dx^2} + J(z)\frac{d}{dx} & J(z)\frac{d}{dx} & T(z)\frac{d}{dx} & P(z)\frac{d}{dx} & R(z)\frac{d}{dx} & 0 & 0 \\ \Delta_1^k(z)_{,z}\frac{d}{dx} & \Delta_2^k(z)_{,z}\frac{d^2}{dx^2} & \Delta_3^k(z)_{,z}\frac{d}{dx} & \Delta_4^k(z)_{,z}\frac{d}{dx} & \Delta_5^k(z)_{,z}\frac{d}{dx} & \Delta_6^k(z)_{,z}\frac{d}{dx} & \Delta_7^k(z)_{,z} & \Delta_8^k(z)_{,z} \\ 0 & J(z)_{,z}\frac{d}{dx} & J(z)_{,z} & T(z)_{,z} & P(z)_{,z} & R(z)_{,z} & 0 & 0 \end{bmatrix}.$$

The displacement vector of the reference layer $\boldsymbol{u}_u$ may be expressed in terms of the nodal variables vector $\boldsymbol{u}_u^e$ as follows:

$$\boldsymbol{u}_u = \boldsymbol{N}_u \boldsymbol{u}_u^e \tag{36}$$

where

$$\boldsymbol{u}_u^e = \big\{ (u_0)_1 \ (w_0)_1 \ \theta_1 \ (w_{0,x})_1 \ (u_1^1)_1 \ (X^+)_1 \ (X^-)_1 \ (Z^+)_1 \ (Z^-)_1 \ (u_0)_3 \ \theta_3 \ (u_1^1)_3 \\ (X^+)_3 \ (X^-)_3 \ (Z^+)_3 \ (Z^-)_3 \ (u_0)_2 \ (w_0)_2 \ \theta_2 \ (w_{0,x})_2 \ (u_1^1)_2 \ (X^+)_2 \ (X^-)_2 \ (Z^+)_3 \ (Z^-)_3 \big\}^T ,$$

$$\boldsymbol{N}_u = \begin{bmatrix} \bar{N}_1 & 0 & 0 & 0 & 0 & 0 & 0 & 0 & 0 & \bar{N}_3 & 0 & 0 & 0 \\ 0 & N_1 & 0 & Nd_1 & 0 & 0 & 0 & 0 & 0 & 0 & 0 & 0 & 0 \\ 0 & 0 & \bar{N}_1 & 0 & 0 & 0 & 0 & 0 & 0 & 0 & \bar{N}_3 & 0 & 0 \\ 0 & 0 & 0 & 0 & \bar{N}_1 & 0 & 0 & 0 & 0 & 0 & 0 & \bar{N}_3 & 0 \\ 0 & 0 & 0 & 0 & 0 & \bar{N}_1 & 0 & 0 & 0 & 0 & 0 & 0 & \bar{N}_3 \\ 0 & 0 & 0 & 0 & 0 & 0 & \bar{N}_1 & 0 & 0 & 0 & 0 & 0 & 0 \\ 0 & 0 & 0 & 0 & 0 & 0 & 0 & \bar{N}_1 & 0 & 0 & 0 & 0 & 0 \\ 0 & 0 & 0 & 0 & 0 & 0 & 0 & 0 & \bar{N}_1 & 0 & 0 & 0 & 0 \end{bmatrix}$$

$$\begin{bmatrix} 0 & 0 & 0 & \bar{N}_2 & 0 & 0 & 0 & 0 & 0 & 0 & 0 & 0 \\ 0 & 0 & 0 & 0 & N_2 & 0 & Nd_2 & 0 & 0 & 0 & 0 & 0 \\ 0 & 0 & 0 & 0 & 0 & \bar{N}_2 & 0 & 0 & 0 & 0 & 0 & 0 \\ 0 & 0 & 0 & 0 & 0 & 0 & 0 & \bar{N}_2 & 0 & 0 & 0 & 0 \\ 0 & 0 & 0 & 0 & 0 & 0 & 0 & 0 & \bar{N}_2 & 0 & 0 & 0 \\ \bar{N}_3 & 0 & 0 & 0 & 0 & 0 & 0 & 0 & 0 & \bar{N}_2 & 0 & 0 \\ 0 & \bar{N}_3 & 0 & 0 & 0 & 0 & 0 & 0 & 0 & 0 & \bar{N}_2 & 0 \\ 0 & 0 & \bar{N}_3 & 0 & 0 & 0 & 0 & 0 & 0 & 0 & 0 & \bar{N}_2 \end{bmatrix}$$

in which $\bar{N}_i$ $(i = 1, 2, 3)$ are the Lagrangian quadratic shape functions defined as:

$$\bar{N}_1 \equiv \bar{N}_1(\xi) = -\xi(1-\xi)/2, \ \bar{N}_2 \equiv \bar{N}_2(\xi) = \xi(1+\xi)/2, \ \bar{N}_3 \equiv \bar{N}_3(\xi) = (1+\xi)(1-\xi)/2, \tag{37}$$

and the Hermitian shape functions are

$$\begin{aligned} N_1 = N_1(\xi) &= \frac{1}{4}(1-\xi)^2(2+\xi), \quad N_2 = N_2(\xi) = \frac{1}{4}(2-\xi)(1+\xi)^2, \\ Nd_1 = Nd_1(\xi) &= \frac{l_e}{8}(1-\xi)^2(1+\xi), \quad Nd_2 = Nd_2(\xi) = -\frac{l_e}{8}(1-\xi)(1+\xi)^2 \end{aligned} \tag{38}$$

where ξ is the natural coordinate and l_e denotes the length of the element. Using Eqs. (35) and (36), the displacement and the strain vectors may be expressed as follows:

$$\mathbf{u} = \mathbf{A}_u \mathbf{u}_u = \mathbf{A}_u \mathbf{N}_u \mathbf{u}_u^e = \mathscr{N} \mathbf{u}_u^e, \tag{39}$$

$$\boldsymbol{\varepsilon} = \boldsymbol{L}_u \boldsymbol{u}_u = \boldsymbol{L}_u \boldsymbol{N}_u \boldsymbol{u}_u^e = \mathscr{B}_u \boldsymbol{u}_u^e. \tag{40}$$

The principle of virtual displacement is employed to extract the governing equations of the beam element. According to this principle, for a mechanical medium with volume Ω and regular boundary surfaces Γ, one may write:

$$\delta\Pi = \delta U - \delta W = \int_\Omega \boldsymbol{\delta\varepsilon}^T \boldsymbol{\sigma} \mathrm{d}\Omega - \int_\Gamma \boldsymbol{\delta u}^T \boldsymbol{F} \mathrm{d}S - \int_\Omega \boldsymbol{\delta u}^T \mathbf{f} \mathrm{d}\Omega - \boldsymbol{\delta u}_c^T \boldsymbol{f}_c + \int_\Omega \rho \boldsymbol{\delta u}^T \ddot{\boldsymbol{u}} \mathrm{d}\Omega = 0 \tag{41}$$

where $\boldsymbol{\delta u}$, $\boldsymbol{F}$, $\boldsymbol{f}$, and $\boldsymbol{f}_c$ are the admissible virtual displacement, traction, body force, and concentrated force vectors, respectively. U, W, and ρ are the strain energy, work of the externally applied loads, and mass density, respectively.

Substituting Eqs. (1), (39) and (40) into Eq. (41), and assembling the element matrices, the following general equations of motion are obtained for the entire beam:

$$\mathscr{M} \ddot{\boldsymbol{u}}(t) + \mathscr{K} \boldsymbol{u}(t) = \mathscr{F}(t) \tag{42}$$

where

$$\mathscr{M} = \int_{\Omega} \rho \mathscr{N}^T \mathscr{N} \mathrm{d}\Omega,$$
$$\mathscr{K} = \int_{\Omega} \mathscr{B}_u^T \bar{\boldsymbol{C}} \mathscr{B}_u \mathrm{d}\Omega,$$
$$\mathscr{F} = \int_{\Omega} \mathscr{N}^T \boldsymbol{f} \mathrm{d}V + \int_{\Gamma} \mathscr{N}^T \boldsymbol{F} \mathrm{d}S + \mathscr{N}^T \boldsymbol{f}_c.$$

4 Results and discussions

In the present Section, static and free vibration analyses of composite beams with different stacking sequences and boundary conditions are considered to evaluate the efficiency and the accuracy of the present theory. Results of the present theory are compared with either previously published results of well-known references or the finite elements results obtained based on the 3D theory of elasticity (ABAQUS and ANSYS softwares). Present results are extracted from a MATLAB program written by the authors based on the proposed refined global-local theory. It is worth mentioning that the proposed beam element has a proper rank, because the exact integration method is employed to calculate the stiffness matrices. Moreover, since comparisons available in literature reveal that results of the global (equivalent single layer) theories and the majority of the available local theories may encounter serious accuracy problems in some circumstances [37–39], results of the present theory have been compared mainly with results obtained based on the three-dimensional theory of elasticity.

4.1 Bending analysis results

4.1.1 A simply supported three-layer [0°/90°/0°] *beam*

In the current example, a three-layered [0°/90°/0°] simply supported composite beam with a length to thickness ratio of $S = 4$ (thick beam) is analyzed using the proposed finite element formulation. The beam is made of carbon/epoxy with the following material properties:

$$(E_L, E_T, G_{LT}, G_{TT}) = (172.4, 6.895, 3.448, 1.379)GPa, (\nu_{LT}, \nu_{TT}) = (0.25, 0.25),$$

L and T denote directions parallel and normal to the fibers, respectively. All layers of the beam have equal thickness. The beam is subjected to a sinusoidal pressure $p = p_0 \sin(\pi x/L)$ on its top surface. The exact solution of the problem has been previously obtained by Pagano [4] based on the three-dimensional theory of elasticity. The accuracy of the results of the present formulation is evaluated by comparing the obtained results with of those of Pagano [4]. The following normalized quantities are used for the mentioned comparison:

$$(\bar{u}, \bar{w}) = E_T(u/hp_0, 100w/hS^3 p_0), (\bar{\sigma}_{xx}, \bar{\sigma}_{zz}, \bar{\tau}_{xz}) = (\sigma_{xx}, \sigma_{zz}, \tau_{xz})/p_0.$$

Due to the symmetry, only half of the beam is modeled. Results of the mesh convergence study are shown in Table 1. This table shows that the convergence rate of the proposed finite element model is very high. Only 2

Table 1 Results of the mesh convergence study for the three-layer [0°/90°/0°] beam with $S = 4$

	Number of the elements					
	2	4	8	12	15	Exact
$\bar{w}(0.5L, 0)$	2.9061	2.9051	2.9051	2.9051	2.9051	2.8872
$\bar{u}(0, 0.5h)$	−9.4651	−9.4616	−9.4614	−9.4614	−9.4614	−9.2097
$\bar{\tau}_{13}(0, 0)$ (C)	1.4205	1.4192	1.4191	1.4191	1.4191	1.4515
$\bar{\tau}_{13}(0, 0)$ (C)	1.2842	1.3789	1.4031	1.4077	1.4090	1.4515
$\bar{\sigma}_{33}(0.5L, 0)$ (E)	0.5	0.5	0.5	0.5	0.5	0.4966
$\bar{\sigma}_{33}(0.5L, 0)$ (E)	0.3396	0.4578	0.4897	0.4982	0.4988	0.4966
$\bar{\sigma}_{11}(0.5L, 0.5h)$	19.8358	19.1757	18.9996	18.9665	18.9570	18.6630

Table 2 $\bar{w}(L/2, 0)$ of the three-layer beam for different values of the length to thickness ratio

S	$\bar{w}(L/2, 0)$		
	Exact	Present	Difference (%)
4	2.8872	2.9051	0.62
10	0.9272	0.9329	0.61
20	0.6173	0.6174	0.02
30	0.5578	0.5577	0.02
40	0.5367	0.5367	0

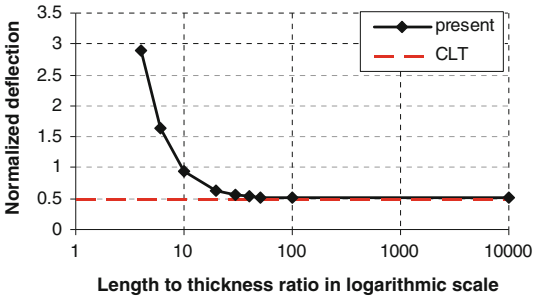

Fig. 4 The normalized transverse deflection versus the aspect ratio for the three-layer beam

elements were adequate to predict the deflection of the beam. A mesh with 4 elements gives excellent results for the in-plane displacement and stress components. The transverse shear and normal stresses have been calculated using two different methods: (i) employing the constitutive equations; (ii) integrating the elasticity equilibrium equations in terms of the stress components, along the thickness of the laminate. Results of these two approaches are denoted by (C) and (E), respectively.

The normalized numerical results for the maximum values of the transverse deflection are given in Table 2 for different length to thickness ratios. It can be deduced from this Table that the present model has predicted the deflection of the laminated beam with an error that is less than *0.65%*. Although the differences are mainly due to using different solution procedures, the present fourth-order approximation of the transverse displacement component has improved the prediction of the deflection of the beam considerably. Variations of the normalized deflection versus the aspect ratio are shown in Fig. 4. A comparison of the present results with results of the classical beam theory (CLT) reveals that the present beam element is free of shear locking.

Through-the-thickness variations of the normalized in-plane displacement and stress components are shown in Fig. 5. It may be readily seen from Fig. 5 that the proposed finite element formulation predicts the in-plane stress very accurately. The transverse shear stress distribution obtained from the equilibrium equations is in better agreement with the exact solution. As it may be expected, the presented refined global-local model predicts the transverse shear stress with sufficient accuracy from the constitutive law (the maximum error is about *4.5%*). The predicted results of the transverse normal stress based on integrating the equilibrium equations agree very well with results of the theory of elasticity. The transverse normal stress calculated based on the constitutive equations is compared well with the elasticity solution with a relative error of *9%*. The obtained results also show that the presented model predicts the in-plane displacement of the thick beam with an error that is less than *5%*. It can be deduced from these results that the proposed finite element model performs very well in the bending analysis of the thick laminated beams.

4.1.2 A simply supported two-layer [0°/90°] beam

A two-layered [0°/90°] simply supported composite beam with a length to thickness ratio of $S = 4$ is analyzed using the proposed refined global-local model to evaluate the accuracy of the proposed model for an asymmetric lamination scheme with an extensional-bending coupling. Material properties and load conditions of the present example are the same as those of the previous example. The 3D exact solution of this case study has been also obtained by Pagano [4].

Results of the mesh convergence study for this example are shown in Table 3. Results of Table 2 show a high convergence rate, due to using the proposed finite element model. For the prediction of the in-plane

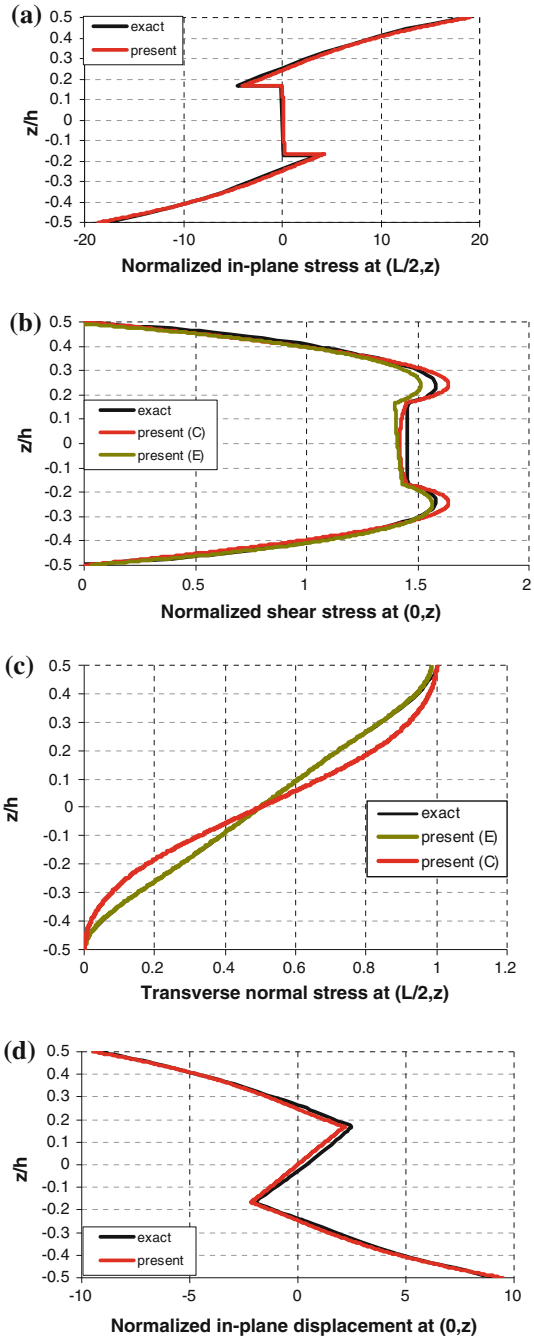

Fig. 5 Through-the-thickness distribution of $\bar{\sigma}_{xx}$, $\bar{\tau}_{xz}$, $\bar{\sigma}_{zz}$, and $\bar{u}$ for the simply supported three-layer beam ($S = 4$)

displacement and stress components, only 4 elements were required. A mesh with 2 elements was adequate to predict the lateral deflection of the thick laminated beam with a less than *0.30%* error.

In Fig. 6, the normalized lateral deflection of the beam versus its aspect ratio is shown. It can be inferred from this figure that the presented beam element is free from shear locking as the element is developed based on a field consistency approach.

Figure 7 depicts variations of the normalized in-plane displacement and stress components along the thickness direction. The prediction of the transverse shear and normal stresses based on the equilibrium equations agrees very well with the exact elasticity solution. The proposed refined global-local model also predicts the in-plane stress very accurately. Similar to the previous case study, the presented finite element model predicts

Table 3 A convergence study by adopting various meshes for the two-layer beam [0°/90°] with $S = 4$

	Number of the elements					
	2	4	8	12	15	exact
$\bar{w}(0.5L, 0)$	4.6827	4.6819	4.6818	4.6818	4.6818	4.6950
$\bar{u}(0, 0.5h)$	−4.8333	−4.8323	−4.8322	−4.8322	−4.8322	−4.5286
$\bar{\tau}_{13}(0, -0.25h)$ (C)	2.5753	2.5719	2.5717	2.5717	2.5717	2.7107
$\bar{\tau}_{13}(0, -0.25h)$ (C)	2.5313	2.7176	2.7654	2.7743	2.7768	2.7107
$\bar{\sigma}_{33}(0.5L, 0)$ (E)	0.7202	0.7281	0.7292	0.7292	0.7292	0.7786
$\bar{\sigma}_{33}(0.5L, 0)$ (E)	0.5420	0.7303	0.7813	0.7909	0.7952	0.7786
$\bar{\sigma}_{11}(0.5L, -0.5h)$	−33.4641	−32.3332	−32.0316	−31.9749	−31.9586	−30.1181

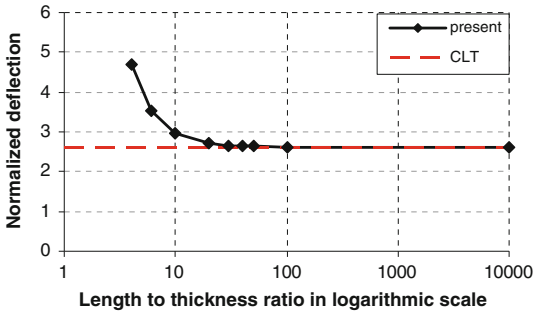

Fig. 6 Variations of the normalized transverse deflection versus the aspect ratio for the two-layer beam

the transverse shear stress of the two-layer beam satisfactorily from the constitutive equations. The obtained results also show that the proposed model predicts the transverse normal stress from the constitutive equations with an error that is less than 8%. The in-plane displacement of the thick beam is compared well with the elasticity solution within a *6.7%*. error.

4.1.3 A four-layer cantilever beam with a symmetric lay-up

A four-layer cantilever beam with a length of $L = 10\ m$ and a unit width is analyzed using the proposed finite element formulation for $S = 4$, 10 and 50 length to thickness ratios. These ratios correspond to thick, relatively thick and thin beams, respectively. Some theories encounter serious accuracy problems when the number of the layers increases. The cantilever beam has a [90°/0°/0°/90°] lamination scheme, and its material properties are similar to those mentioned in Section 4.1.1. The laminated beam is subjected to a distributed uniform pressure Z^+ on its top surface, and shear tractions X^+ and X^- on its top and bottom surfaces, respectively (Fig. 8). In the analysis of the beam with length to thickness ratio $S = 4$, values $Z^+ = 100\ \mathrm{N/m^2}$, $X^+ = 500\ \mathrm{N/m^2}$ and $X^- = -500\ \mathrm{N/m^2}$ are assumed for the applied loads. In $S = 10$ and $S = 50$ cases these values are adopted as ($Z^+ = 100\ \mathrm{N/m^2}$, $X^+ = 1250\ \mathrm{N/m^2}$, $X^- = -1250\ \mathrm{N/m^2}$) and ($Z^+ = 100\ \mathrm{N/m^2}$, $X^+ = 6250\ \mathrm{N/m^2}$, $X^- = -6250\ \mathrm{N/m^2}$), respectively. Since no exact 3D solution is available for the considered example, a 3D finite element analysis was performed in ABAQUS with a very refined mesh, using the 20-node C3D20R solid element.

In order to analyze the problem, the beam was mathematically discretized into 20 beam elements of equal lengths. For different values of the length to thickness ratio, the maximum transverse deflections are given in Table 4. The obtained results have a good agreement with results obtained from ABAQUS. It can be concluded from this Table that the present refined global-local model predicts the deflection of the thin and moderately thick laminated beams with an error that is less than *2.5%*.

To assess the accuracy of the present model in predicting the local variations, variations of the stress components are depicted in Fig. 9 for the thick beam ($S = 4$). Although in case of homogenous boundary conditions of the shear stresses the presented model can estimate transverse shear stresses well from the constitutive equations, an accurate and reliable prediction of them in case of non-zero boundary shear tractions requires integrating the equilibrium equations. It may be easily seen from Fig. 9 that the depicted stress components are correlated well with ABAQUS results.

In $S = 10$ and $S = 50$ cases, the through-the-thickness distribution of the stress components and the in-plane displacement along the thickness direction are shown in Figs. 10 and 11. These figures show that the

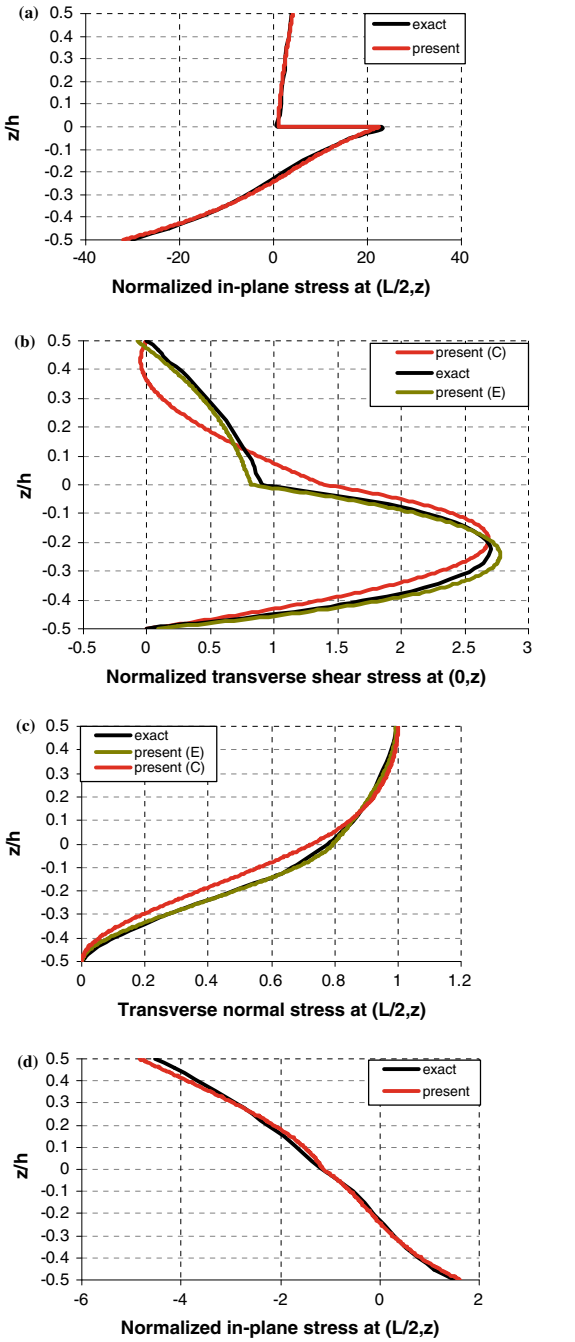

Fig. 7 Through-the-thickness distribution of $\bar{\sigma}_{xx}$, $\bar{\tau}_{xz}$, $\bar{\sigma}_{zz}$ and $\bar{u}$ for the simply supported two-layer beam ($S = 4$)

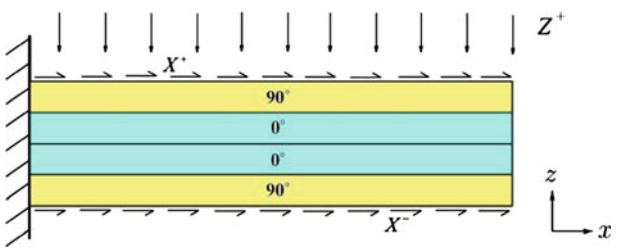

Fig. 8 Description of the geometry, boundary conditions and loadings of the [90°/0°/0°/90°] beam

Table 4 $w(L,0)$of the clamped $[90°/0°/0°/90°]$ beam for different S ratios

S	$w(L,0)$		
	ABAQUS	Present	Difference (%)
4	-4.5829×10^{-6}	-4.0816×10^{-6}	10.94
10	-5.7154×10^{-5}	-5.5787×10^{-5}	2.39
50	-6.8018×10^{-3}	-6.7884×10^{-3}	0.20

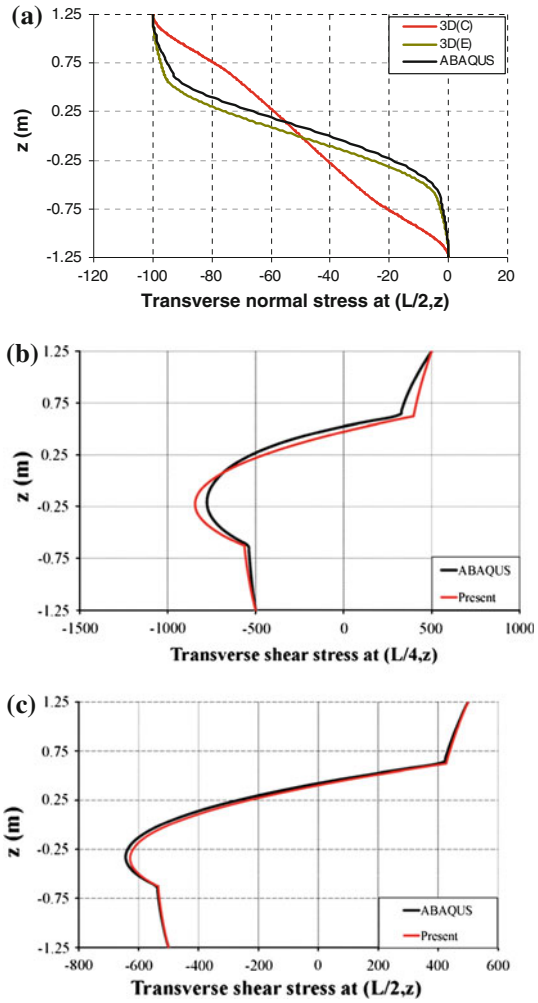

Fig. 9 Through-the-thickness variations of $\sigma_{zz}(N/m^2)$ and $\tau_{xz}(N/m^2)$ for the clamped $[90°/0°/0°/90°]$ beam with $S = 4$

new finite element model performs very well in the prediction of the transverse shear and normal stresses. Concerning the in-plane stress, the obtained results are also good. The maximum error in the case of a moderately thick beam is approximately *7.5%*. For higher S values, the error has reduced significantly. The present model predicts the in-plane displacement of the thin to moderately thick beams within a *6.5%* error. These results show that the present laminated beam model is suitable for predicting behaviors of the composite laminated beams under non-homogenous shear and normal traction boundary conditions.

4.1.4 A four-layer cantilever beam with an anti-symmetric lay-up

Geometry, material properties, and boundary and loading conditions of the laminated composite beam of the present example are the same as those of the previous Section. The only difference is that the considered beam has an asymmetric $[0°/90°/0°/90°]$ lay-up.

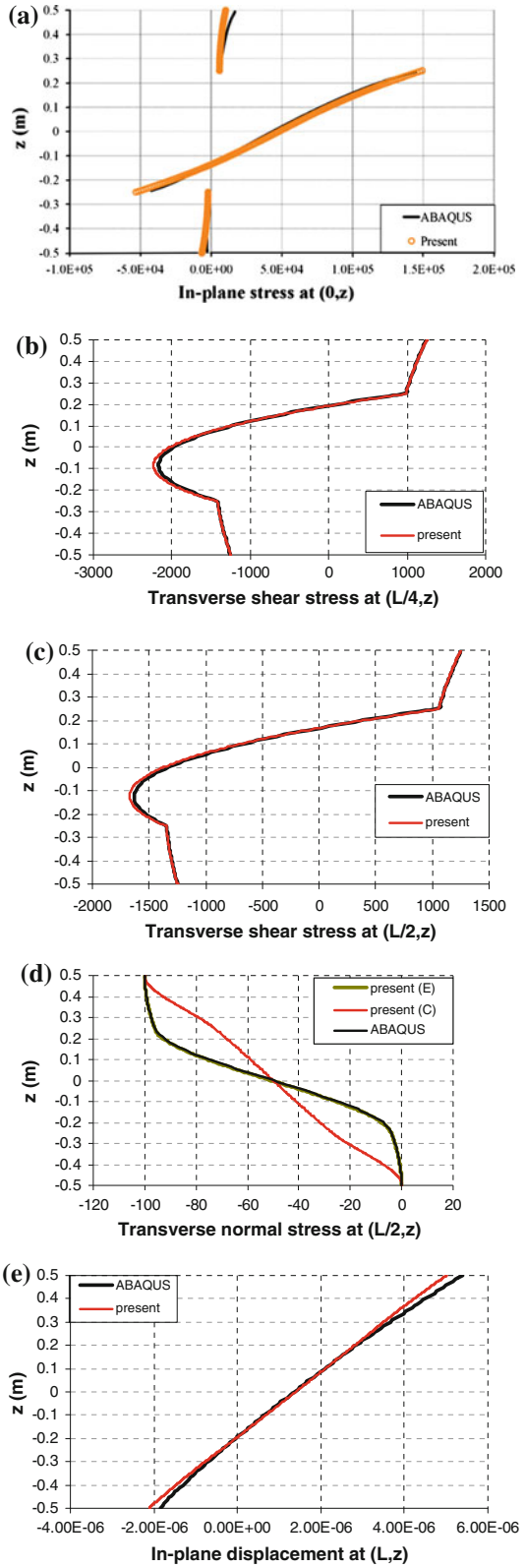

Fig. 10 Through-the-thickness distribution of $\sigma_{xx}(N/m^2)$, $\tau_{xz}(N/m^2)$, $\sigma_{zz}(N/m^2)$ and $u(m)$ for the clamped $[90°/0°/0°/90°]$ beam with $S = 10$

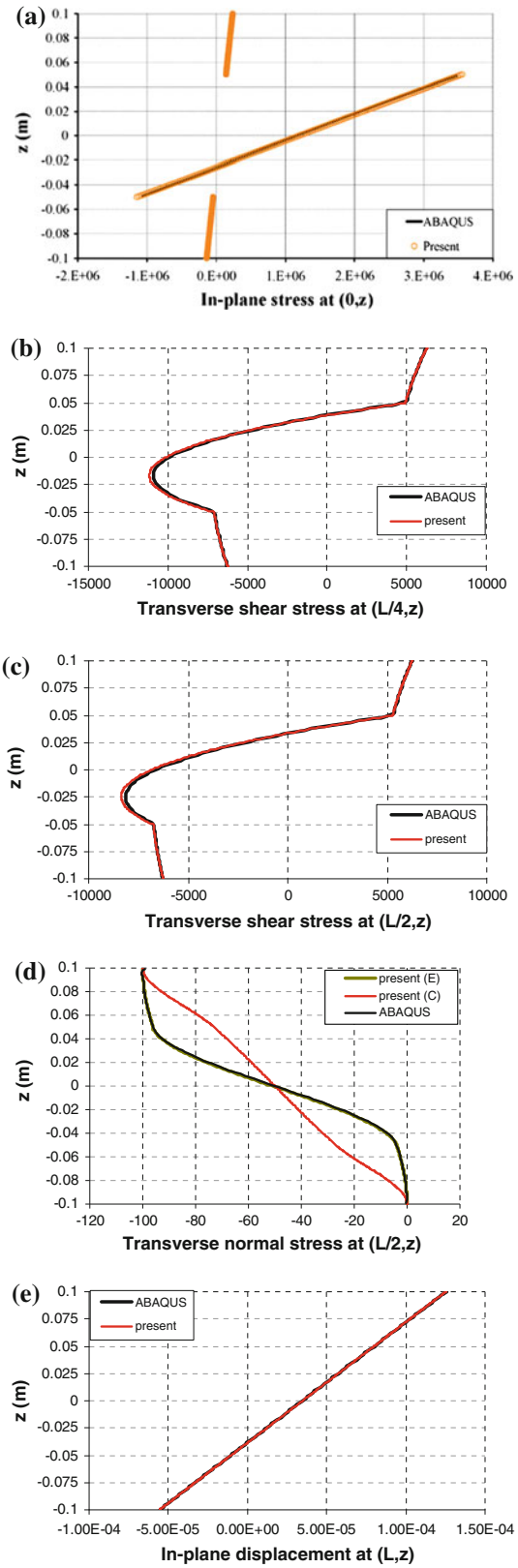

Fig. 11 Through-the-thickness variations of $\sigma_{xx}(N/m^2)$, $\tau_{xz}(N/m^2)$, $\sigma_{zz}(N/m^2)$ and $u(m)$ for the clamped $[90°/0°/0°/90°]$ beam with $S = 50$

The through-the-thickness distribution of the transverse shear and normal stresses are depicted in Fig. 12 for the relatively thick beam ($S = 10$). The obtained results agree well with those of the ABAQUS solution. It can be seen from Fig. 12 that the model predicts the transverse shear and normal stresses very accurately. Since fibers of the top surface are in the longitudinal direction, it is expected that the stress components and, consequently, the in-plane displacements of the outermost layers become smaller than in the previous case. The obtained results also confirm this idea. The maximum values of lateral deflection are given in Table 5 for different values of the length to thickness ratio. As in the previous example, for higher values of S, the discrepancies reduce significantly. The obtained results confirm the efficiency of the proposed new finite element formulation for the bending analysis of laminated beams with non-homogenous normal and shear traction boundary conditions.

4.1.5 A three-layer sandwich beam with a soft core

As a final example in the bending analysis, a three-layer sandwich beam with a soft core is considered. In this case, results of the majority of the available theories may become unreliable due to neglecting the continuity conditions of the transverse shear and normal stress components at the layer interfaces, and ignoring effects of the transverse flexibility and the normal stress. In this regard, a simply-supported sandwich beam with length $L = 10$ m, cross section width $b = 1$ m, and length to thickness ratio $S = 4$ is considered. The thickness of each face sheet is 0.1 h, and the thickness of the soft core is 0.8 h. The face sheets are made of graphite-epoxy with the following material properties:

$$(E_{11}, E_{22}, E_{33}, G_{12}, G_{13}, G_{23}) = (131.1, 6.9, 6.9, 3.588, 3.088, 2.3322)\ \text{GPa},\ (\nu_{12}, \nu_{13}, \nu_{23}) = (0.32, 0.32, 0.49).$$

The material of the core is a DivingH60 Cell with the following material properties [49]:

$$E_c = 56\ \text{MPa},\ \nu_c = 0.27.$$

The sandwich beam is subjected to uniform pressures $Z^+ = -500\ \text{N/m}^2$ and $Z^- = 500\ \text{N/m}^2$.

Through-the-thickness distributions of the in-plane and transverse shear stresses are plotted in Fig. 13. In Fig. 14, through-the-thickness distributions of the transverse normal stress and lateral displacement are shown. These results are compared with results of the 3D finite element analysis (ABAQUS) as a benchmark. It may be observed that the depicted stress components based on the present formulation are in excellent agreement with those extracted from the 3D finite element analysis. It may be readily noted that the proposed refined global-local model predicts the through-thickness changes of the transverse displacement with an error that is less than *5%*. These results confirm the accuracy of the proposed formulation for a bending analysis of the sandwich beams.

4.2 Free vibration analysis

4.2.1 Free vibration of a laminated composite beam

A free vibration analysis of a simply supported composite cross-ply [0°/90°/90°/0°] beam with a length to thickness ratio of $S = 10$ and 20 is carried out using the proposed refined global-local finite element model. The beam is made of a material with the following properties:

$$(E_L, E_T, G_{LT}, G_{TT}) = (181, 10.3, 7.17, 2.87)\text{GPa},\ (\nu_{LT}, \nu_{TT}) = (0.25, 0.33),\ \rho = 1578\ \text{kg/m}^3.$$

Before performing the free vibration validation analysis, a convergence study with respect to the mesh size is carried out for the aspect ratio $S = 10$. Table 6 shows the high convergence rate of the proposed finite element model. It can be deduced from this Table that a mesh with 10 elements is sufficient to model the laminated composite beam behavior for a dynamic analysis.

Table 7 presents the first natural frequencies for length to thickness ratios $S = 10$ and 20. These results are presented in terms of the following non-dimensional natural frequency:

$$\bar{\omega} = \omega L S (\rho / E_T)^{1/2}.$$

The mode shapes of the moderately thick beam ($S = 10$) are shown in Fig. 15. A description of the modes is given in Table 7. For comparison purposes, results of both 3D finite element (ANSYS) [33] and exact 2D [50]

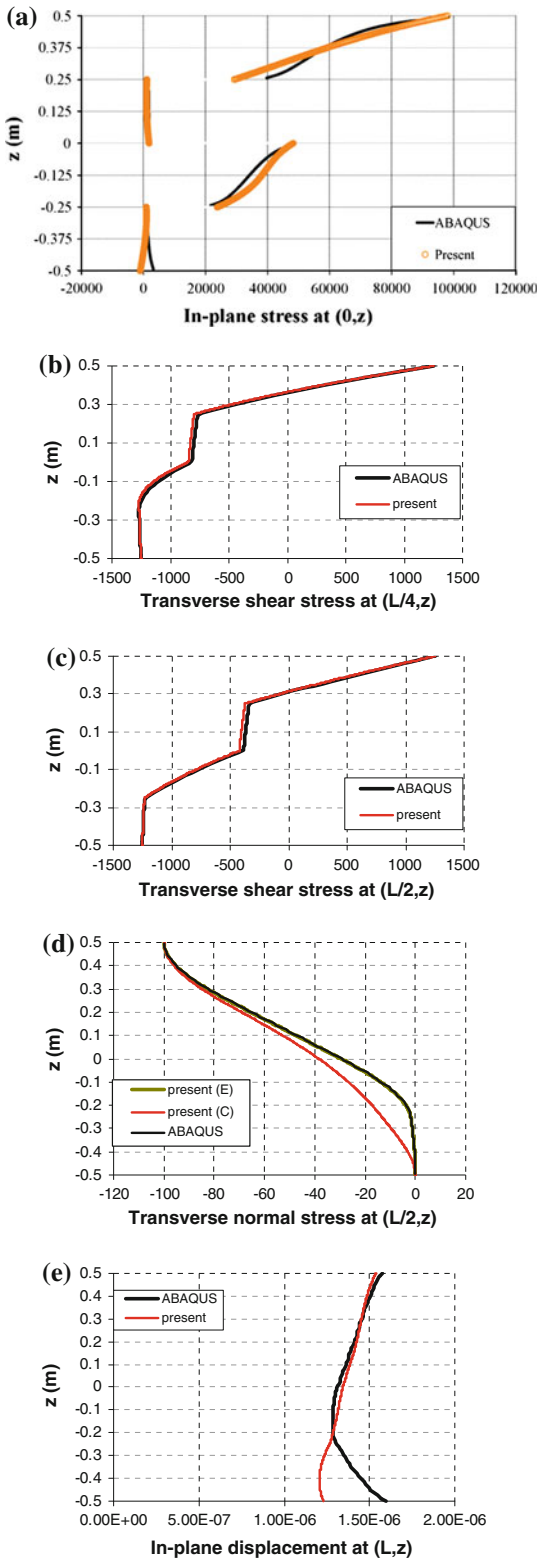

Fig. 12 Variations of $\sigma_{xx}(N/m^2)$, $\tau_{xz}(N/m^2)$, $\sigma_{zz}(N/m^2)$ and $u(m)$ through the thickness for the $[0°/90°/0°/90°]$ beam $(S=10)$

Table 5 $w(L,0)$ of the clamped [0°/90°/0°/90°] beam for different S values

S	$w(L,0)$		
	ABAQUS	Present	Difference (%)
4	-0.9140×10^{-6}	-1.1821×10^{-6}	29.33
10	-6.2601×10^{-6}	-7.0435×10^{-6}	12.51
50	-5.8244×10^{-4}	-5.8591×10^{-4}	0.60

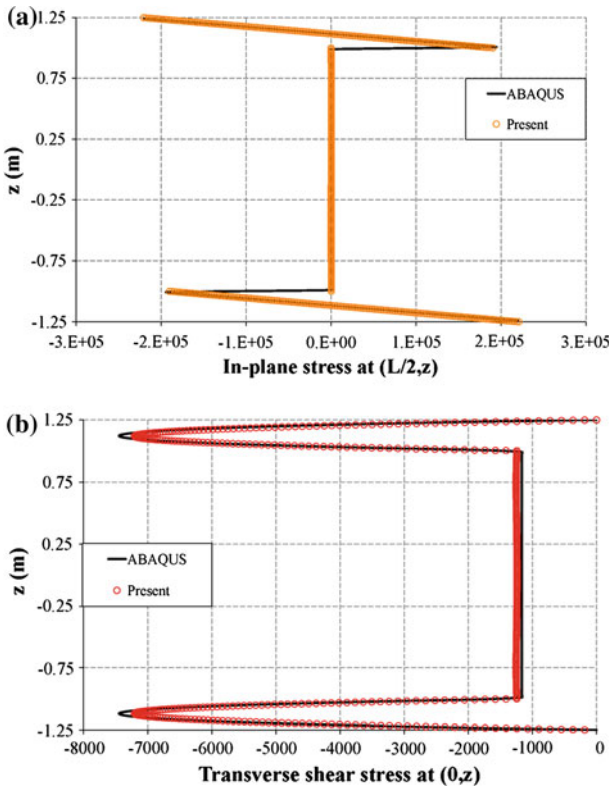

Fig. 13 Variations of σ_{xx} and τ_{xz} along the thickness direction for a sandwich beam with a soft core ($S = 4$)

solutions have been employed. Table 7 shows that results of the proposed finite element model agree well with the exact values. The discrepancy in the first five non-dimensional natural frequencies of the relatively thick beam is less than *2%*. The present model predicts the first seven non-dimensional frequencies of the relatively thin beam within a *1%* error.

4.2.2 Free vibration of a three-layer sandwich beam

In this example, three-layer simply supported sandwich beams with length to thickness ratios S = 10 and 20 are considered. The thickness of each face sheet is 0.1h, and the thickness of the core is 0.8h. The face sheets are made of graphite-epoxy with the following material properties:

$$(E_{11}, E_{22}, E_{33}, G_{12}, G_{13}, G_{23}) = (131.1, 6.9, 6.9, 3.588, 3.088, 2.3322)\ \text{GPa}.$$

The material properties of the core are:

$$(E_{11}, E_{22}, E_{33}, G_{12}, G_{13}, G_{23}) = (0.2208, 0.2001, 2760, 16.56, 545.1, 455.4)\ \text{MPa}$$
$$(\nu_{12}, \nu_{13}, \nu_{23}) = (0.99, 0.00003, 0.00003), \quad \rho_c = 70\ \text{Kg/m}^3.$$

Similar to the previous example, results are presented in terms of the following non-dimensional natural frequency:

$$\bar{\omega} = \omega L S (\rho_f / E_0)^{1/2}$$

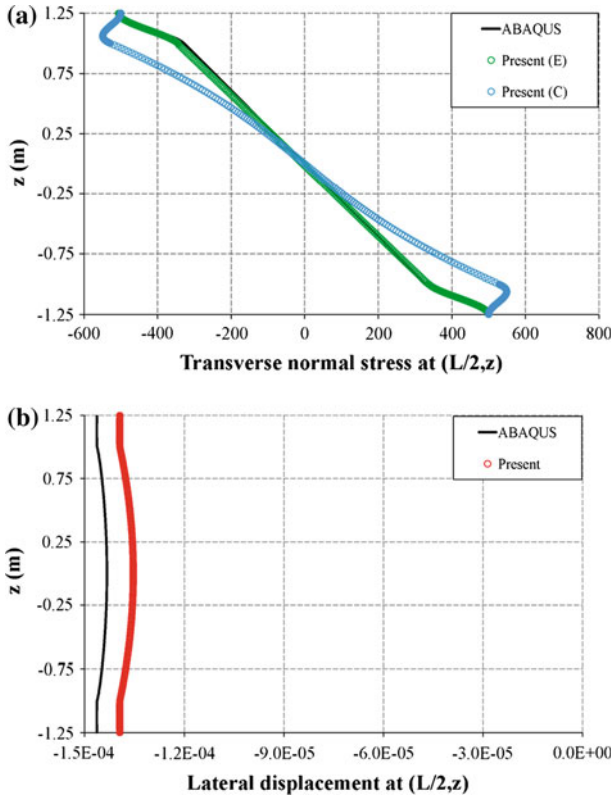

Fig. 14 Through-the-thickness variations of σ_{zz} and w for a sandwich beam with a soft core ($S = 4$)

Table 6 A convergence test based on the obtained non-dimensional natural frequencies of the four-layer [0°/90°/90°/0°] beam with $S = 10$

Mode No.	Number of the elements						Exact 2D [50]
	5		10		20		
	$\bar{\omega}$	Error (%)	$\bar{\omega}$	Error (%)	$\bar{\omega}$	Error (%)	$\bar{\omega}$
1	9.37	0.32	9.37	0.32	9.37	0.32	9.34
2	27.30	0.29	27.28	0.22	27.28	0.22	27.22
3	46.41	0.02	46.31	0.24	46.31	0.24	46.42
4	65.74	0.48	65.40	1	65.38	1.03	66.06
5	–	–	84.45	2	84.38	2.08	86.17
6	–	–	103.32	3.21	103.17	3.35	106.75

Table 7 Natural frequencies of the four-layer [0°/90°/90°/0°] beam

S	Non-dimensional natural frequencies $\bar{\omega}$				
	Mode type	Present	Error (%)	ANSYS [33]	Exact 2D [50]
10	Bending	9.37	0.32	9.34	9.34
	Bending	27.28	0.22	27.24	27.22
	Bending	46.31	0.24	46.47	46.42
	Bending	65.40	1	66.19	66.06
	Bending	84.45	2	86.43	86.17
	Axial	95.90	2.26	93.78	–
	Bending	103.32	3.21	107.20	106.75
20	Bending	10.67	0.28	10.64	10.64
	Bending	37.50	0.35	37.40	37.37
	Bending	71.99	0.35	71.85	71.74
	Bending	109.21	0.29	109.15	108.89
	Bending	147.27	0.16	147.54	147.04
	Bending	185.63	0.03	186.53	185.68
	Axial	191.88	0.71	190.52	–

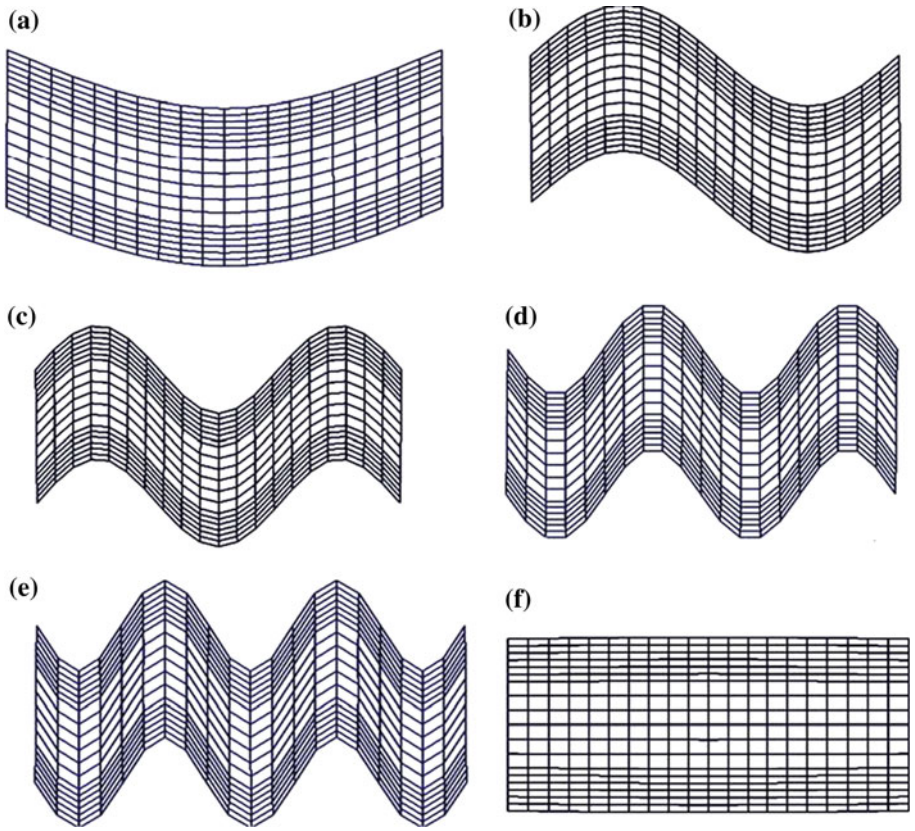

Fig. 15 Mode shapes of the four-layer [0°/90°/90°/0°] beam with $S = 10$ (description of the modes are given in Table 7)

Table 8 Natural frequencies of the sandwich beam

S	Non-dimensional natural frequencies $\bar{\omega}$				
	Mode type	Present	Difference (%)	ANSYS [33]	Exact 2D [50]
10	Bending	12.52	2.37	12.23	12.23
	Bending	32.11	2.62	31.30	31.29
	Bending	50.76	1.10	50.26	50.21
	Bending	68.05	0.06	69.21	68.09
	Bending	83.97	4.77	88.41	88.18
	Axial	121.37	1.12	120.03	–
20	Bending	15.55	1.11	15.38	15.38
	Bending	50.07	2.31	48.98	48.94
	Bending	89.32	2.78	87.01	86.90
	Bending	166.41	2.02	163.58	163.12
	Bending	203.05	1.09	201.64	200.87
	Axial	242.74	0.47	241.61	–

where $E_0 = 6.9$ GPa. The dimensionless first six natural frequencies of the sandwich beam are given in Table 8. The present model was able to predict the first six non-dimensional frequencies of the relatively thick sandwich beam with a maximum difference of *5%*. In case of a relatively thin beam, the error was less than *3%*.

These results prove the efficiency of the proposed refined global-local model for the free vibration analysis of the laminated composite and sandwich beams.

5 Conclusions

A computationally economic and accurate refined global-local finite element model is presented for bending and vibration analyses of the laminated composite/sandwich beams. In contrast to the available theories, all

the kinematic and stress boundary conditions are satisfied at the layers interfaces. Moreover, the transverse normal stress and the transverse flexibility of the beam are taken into account. The global part of the describing expressions of the in-plane displacements of the beam contains either a high-order polynomial or a combination of a high-order polynomial and an exponential expression whereas the local expressions are adopted either on layerwise or discrete-layer concepts. In contrast to the available laminated composite beam models, the non-uniform nonzero shear and normal traction boundary conditions of the top and bottom surfaces of the beam are also satisfied. In the proposed finite element formulation, the number of the unknown parameters is very small and is independent of the number of the layers. Besides, the shear locking phenomenon does not appear in the presented beam element.

In order to verify the accuracy of the proposed finite element formulation, some comparisons have been made with results of the well-known references and results of the three-dimensional theory of elasticity. To this end, both bending and vibration tests are considered for beams with different geometric parameters, stacking sequences, boundary conditions and number of layers. The comparisons show that the presented finite element formulation, besides its advantages of low computational time due to using a small number of the unknown parameters, is sufficiently accurate in modeling of the thin and thick laminated composite beams under different mechanical loading conditions.

References

1. Carrera, E., Brischetto, S.A.: Survey with numerical assessment of classical and refined theories for the analysis of sandwich plates. Appl. Mech. Rev. **62**(010803), 1–17 (2009)
2. Zhang, Y.X., Yang, C.H.: Recent developments in finite element analysis for laminated composite plates. Compos. Struct. **88**, 147–157 (2009)
3. Hu, H., Belouettar, S., Potier-Ferry, M., Daya, E.M.: Review and assessment of various theories for modeling sandwich composites. Compos. Struct. **84**, 282–292 (2008)
4. Pagano, N.J.: Exact solutions for composite laminates in cylindrical bending. J. Compos. Mater. **3**, 398–411 (1969)
5. Pagano, N.J.: Exact solutions for rectangular bi-direction composites and sandwich plates. J. Compos. Mater. **4**, 20–34 (1970)
6. Pagano, N.J., Hatfield, S.J.: Elastic behavior of multilayered bidirectional composites. AIAA J. **10**, 931–9331 (1972)
7. Stavsky, Y., Loewy, R.: On vibrations of heterogeneous orthotropic shells. J. Sound Vibr. **15**, 235–236 (1971)
8. Reissner, E.: The effects of transverse shear deformation on the bending of elastic plates. J. Appl. Mech. **12**, 69–76 (1945)
9. Mindlin, R.D.: Influence of rotatory inertia and shear in flexural motions of isotropic elastic plates. ASME J. Appl. Mech. **18**, 1031–1036 (1951)
10. Whitney, J.M.: The effects of transverse shear deformation on the bending of laminated plates. J. Compos. Mater. **3**, 534–547 (1969)
11. Reddy, J.N.: Mechanics of laminated composite plates and shells: Theory and analysis. 2nd edn. CRC Press, Boca Raton (2004)
12. Reddy, J.N.: A generalization of two-dimensional theories of laminated composite plates. Commun. Appl. Numer. Meth. **3**, 173–180 (1987)
13. Reddy, J.N., Barbero, E.J., Teply, J.: A plate bending element based on a generalized laminate plate theory. Int. J. Numer. Meth. Eng. **28**, 2275–2292 (1989)
14. Barbero, E.J., Reddy, J.N., Teply, J.: An accurate determination of stresses in thick laminates using a generalized plate theory. Int. J. Numer. Meth. Eng. **29**, 1–14 (1990)
15. Robbins, D.H. Jr., Reddy, J.N.: Modeling of thick composites using a layerwise laminate theory. Int. J. Numer. Meth. Eng. **36**, 655–677 (1993)
16. Heuer, R.: Static and dynamic analysis of transversely isotropic, moderately thick sandwich beams by analogy. Acta Mech. **91**, 1–9 (1992)
17. Adam, C., Ziegler, F.: Forced flexural vibrations of elastic-plastic composite beams with thick layers. Compos. Part B **28**, 201–213 (1997)
18. Adam, C.: Moderately large vibrations of imperfect elastic-plastic composite beams with thick layers. Int. J. Acoustics Vib. **7**, 11–20 (2002)
19. Adam, C.: Nonlinear flexural vibrations of layered panels with initial imperfections. Acta Mech. **181**, 91–104 (2006)
20. Lekhnitskii, S.G.: Strength calculation of composite beams. Vestnik inzhen i tekhnikov, No 9 (1935)
21. Ren, J.G.: Bending theory of laminated plates. Compos. Sci. Tech. **27**, 225–248 (1986)
22. Ren, J.G., Owen, D.R.J.: Vibration and buckling of laminated plates. Int. J. Solids Struct. **25**, 95–106 (1989)
23. Ambartsumian, S.A.: Theory of anisotropic plates. Translated from Russian by Cheron T and Edited by Ashton JE., Tech. Pub. Co. (1969)
24. Whitney, J.M.: The effects of transverse shear deformation on the bending of laminated plates. J. Compos. Mater. **3**, 534–547 (1969)
25. Icardi, U.: Eight-noded zig-zag element for deflection and stress analysis of plates with general lay-up. Compos. Part B **29**, 425–441 (1998)
26. Icardi, U.: Higher-order zig-zag model for analysis of thick composite beams with inclusion of transverse normal stress and sublaminates approximations. Compos. Part B **32**, 343–354 (2001)
27. Icardi, U.: A three-dimensional zig-zag theory for analysis of thick laminated beams. Compos. Struct. **52**, 123–135 (2001)

28. Reissner, E.: On a mixed variational theorem and on a shear deformable plate theory. Int. J. Numer. Meth. Eng. **23**, 193–198 (1986)
29. Murakami, H.: A laminated beam theory with interlayer slip. J. Appl. Mech. **51**, 551–559 (1984)
30. Murakami, H.: Laminated composite plate theory with improved in-plane responses. J. Appl. Mech. **53**, 661–666 (1986)
31. Carrera, E.: A study of transverse normal stress effects on vibration of multilayered plates and shells. J. Sound Vibr. **225**, 803–829 (1999)
32. Carrera, E.: Single-layer vs multi-layers plate modeling on the basis of Reissner's mixed theorem. AIAA J. **38**, 342–343 (2000)
33. Vidal, P., Polit, O.: A family of sinus finite elements for the analysis of rectangular laminated beams. Compos. Struct. **84**, 56–72 (2008)
34. Beheshti-Aval, S.B., Lezgy-Nazargah, M.: A finite element model for composite beams with piezoelectric layers using a sinus model. J. Mech. **26**, 249–258 (2010)
35. Carrera, E.: Historical review of Zig-Zag theories for multilayered plates and shells. Appl. Mech. Rev. **56**, 287–308 (2003)
36. Li, X., Liu, D.: Generalized laminate theories based on double superposition hypothesis. Int. J. Numer. Meth. Eng. **40**, 1197–1212 (1997)
37. Shariyat, M.: Non-linear dynamic thermo-mechanical buckling analysis of the imperfect sandwich plates based on a generalized three-dimensional high-order global–local plate theory. Compos. Struct. **92**, 72–85 (2010)
38. Shariyat, M.: A generalized high-order global–local plate theory for nonlinear bending and buckling analyses of imperfect sandwich plates subjected to thermo-mechanical loads. Compos. Struct. **92**, 130–143 (2010)
39. Shariyat, M.: A generalized global–local high-order theory for bending and vibration analyses of sandwich plates subjected to thermo-mechanical loads. Int. J. Mech. Sci. **52**, 495–514 (2010)
40. Carrera, E., Brischetto, S.: Analysis of thickness locking in classical, refined and mixed multilayered plate theories. Compos. Struct. **82**, 549–562 (2008)
41. Lo, K.H., Christensen, R.M., Wu, E.M.: A high-order theory of plate deformation, Part II: Laminated plates. J. Appl. Mech. **44**, 663–676 (1977)
42. Manjunatha, B.S., Kant, T.: New theories for symmetric/unsymmetric composite and sandwich beams with C^0 finite elements. Compos. Struct. **23**, 61–73 (1993)
43. Reddy, J.N.: Theory and Analysis of Elastic Plates and Shells, 2nd ed. CRC/Taylor & Francis, London (2007)
44. Shariyat, M.: Dynamic thermal buckling of suddenly heated temperature-dependent FGM cylindrical shells, under combined axial compression and external pressure. Int. J. Solids Struct. **45**, 2598–2612 (2008)
45. Shariyat, M.: Dynamic buckling of suddenly loaded imperfect hybrid FGM cylindrical shells with temperature-dependent material properties under thermo-electro-mechanical loads. Int. J. Mech. Sci. **50**, 1561–1571 (2008)
46. Shariyat, M.: Dynamic buckling of imperfect laminated plates with piezoelectric sensors and actuators subjected to thermo-electro-mechanical loadings, considering the temperature-dependency of the material properties. Compos. Struct. **88**, 228–239 (2009)
47. Shariyat, M.: Vibration and dynamic buckling control of imperfect hybrid FGM plates with temperature-dependent material properties subjected to thermo-electro-mechanical loading conditions. Compos. Struct. **88**, 240–252 (2009)
48. Polit, O., Touratier, M., Lory, P.: A new eight-node quadrilateral shear bending plate finite element. Int. J. Numer. Meth. Eng. **37**, 387–411 (1994)
49. Bekuit, J.-J.R.B., Oguamanam, D.C.D., Damisa, O.: A quasi-2D finite element formulation for the analysis of sandwich beams. Finite Elem. Anal. Des. **43**, 1099–1107 (2007)
50. Kapuria, S., Dumir, P.C., Jain, N.K.: Assessment of zigzag theory for static loading, buckling, free and forced response of composite and sandwich beams. Compos. Struct. **64**, 317–327 (2004)